PNAS Nexus

PNAS Nexus, 2022, **1**, 1–14
https://doi.org/10.1093/pnasnexus/pgac198
Advance access publication date: 22 October 2022
Research Report

Targeting an evolutionarily conserved "E-L-L" motif in spike protein to identify a small molecule fusion inhibitor against SARS-CoV-2

Indrani Das Jana[a,1], Prabuddha Bhattacharya[b,1], Karthick Mayilsamy[c,d,2], Saptarshi Banerjee[a,2], Gourab Bhattacharje[e], Sayan Das[a], Seemanti Aditya[a], Anandita Ghosh[c], Andrew R. McGill[c,d,f], Syamanthak Srikrishnan[e], Amit Kumar Das[e], Amit Basak[g], Shyam S. Mohapatra[d,f], Bala Chandran[c], Devesh Bhimsaria[h], Subhra Mohapatra[c,d,*], Arunava Roy[c,*] and Arindam Mondal[a,*]

[a]School of Bioscience, Indian Institute of Technology Kharagpur, Kharagpur 721302, India
[b]Department of Chemistry, Mrinalini Datta Mahavidyapith, Kolkata 700051, India
[c]Department of Molecular Medicine, University of South Florida, Tampa, FL 33620, USA
[d]Department of Veterans Affairs, James A Haley Veterans Hospital, Tampa, FL 33612, USA
[e]Department of Biotechnology, Indian Institute of Technology Kharagpur, Kharagpur 721302, India
[f]Department of Internal Medicine, University of South Florida, Tampa, FL 33620, USA
[g]Division of Chemical Science, Indian Institute of Science Education and Research, Kolkata, Mohanpur 741246, India
[h]Department of Bioscience and Bioengineering, Indian Institute of Technology Roorkee, Roorkee 247667, India
*To whom correspondence should be addressed: Email: smohapa2@usf.edu; arunavaroy@usf.edu; arindam.mondal@iitkgp.ac.in
[1]I.D.J. and P.B. contributed equally.
[2]K.M. and S.B. contributed equally.
Edited By: Karen E. Nelson

Abstract

As newer variants of SARS-CoV-2 continue to pose major threats to global human health and economy, identifying novel druggable antiviral targets is the key toward sustenance. Here, we identify an evolutionarily conserved "Ex_3Lx_6L" ("E-L-L") motif present within the HR2 domain of all human and nonhuman coronavirus spike (S) proteins that play a crucial role in stabilizing its postfusion six-helix bundle (6-HB) structure and thus, fusion-mediated viral entry. Mutations within this motif reduce the fusogenicity of the S protein without affecting its stability or membrane localization. We found that posaconazole, an FDA-approved drug, binds to this "E-L-L" motif and impedes the formation of 6-HB, thus effectively inhibiting SARS-CoV-2 infection in cells. While posaconazole exhibits high efficacy in blocking S protein-mediated viral entry, mutations within the "E-L-L" motif rendered the protein completely resistant to the drug, establishing its specificity toward this motif. Our data demonstrate that posaconazole restricts early stages of infection through specific inhibition of membrane fusion and viral genome release into the host cell and is equally effective toward all major variants of concerns of SARS-CoV-2, including Beta, Kappa, Delta, and Omicron. Together, we show that this conserved essential "E-L-L" motif is an ideal target for the development of prophylactic and therapeutic interventions against SARS-CoV-2.

Keywords: SARS-CoV-2spike protein, six-helix bundle 6-HB, fusion inhibitor, Antiviral drug, posaconazole

Significance Statement:

Enveloped viruses mediates fusion of virus and host membranes in order to release their genetic materials into the host cells. Hence, fusion inhibitory drugs are well accepted for their potential to act as effective antivirals against enveloped viruses. Here, we report the discovery of a unique structural motif present across all known coronavirus spike proteins and establish its indispensable role in the fusion process. Subsequently, we exploit this conserved motif as an antiviral target to identify an FDA-approved drug, posaconazole, that can efficiently block membrane fusion, SARS-CoV-2 entry, and infection in human cells. We propose posaconazole as a prime candidate for further evaluations to determine its potential use both as a prophylactic and therapeutic drug against SARS-CoV-2 infection.

Introduction

The COVID-19 pandemic, caused by the severe acute respiratory syndrome coronavirus 2 (SARS-CoV-2), has exposed the global unpreparedness in controlling infectious outbreaks caused by coronaviruses (1). Though vaccines and repurposed drugs are being administered through emergency use authorization (2), the world is still suffering from consecutive waves of the pandemic caused by newer variants of SARS-CoV-2 (3). To outcompete this rapidly evolving pathogen, it is crucial to develop new intervention strategies by focusing on highly conserved molecular targets present

Competing Interest: The authors declare no competing interest.
Accepted: October 18, 2022

within the virus, which will target both the current as well as any forthcoming variants.

In viruses of the Coronaviridae family, the spike protein is responsible for receptor recognition and membrane fusion leading to the release of the viral genomic RNA into the host cell, which makes it a prime target for the development of novel intervention strategies (4, 5). The 1273 aa SARS-CoV-2 S is proteolytically cleaved into two different subunits, S1 and S2 (Figure 1A), where the S1 subunit consists of an N-terminal and a receptor-binding domain, which is responsible for binding to the cell surface ACE2 receptors. The S2 subunit consists of the fusion peptide (FP), heptapeptide repeat sequences 1 and 2 (HR1 and HR2), transmembrane domain, and the cytoplasmic domain, which together drives membrane fusion (6). On the virion surface, the S protein exists as a homotrimer where the S1 and S2 fragments remain noncovalently attached in a prefusion metastable conformation (7). Upon host cell receptor binding, the S2 subunit undergoes major structural rearrangements from the prefusion to a postfusion conformation, which results in protrusion of the hydrophobic FP into the host cell membrane, close juxtaposition of the viral and host cell membranes, and finally fusion of the two membranes together (8).

In the S trimer, the HR1 and HR2 helices from three different S2 subunits interact with each other to form a rod-shaped six-helix bundle (6-HB), also known as "fusion-core." In the 6-HB, three parallel HR1 helices from three individual protomers form a trimeric coiled-coil hydrophobic core around which the HR2s fold back and intertwine in an antiparallel manner (9) participating in a series of intra- as well as intermolecular interactions. These interactions are critical for the stability of the postfusion conformation and are therefore vital for the membrane fusion process (6). This is why peptides that competitively inhibit HR1–HR2 interactions can effectively block 6-HB formation and hence, viral fusion (9–15). Although these studies highlight the importance of the noncovalent interactions in the fusion process, the use of peptides as an effective therapeutic drug has several limitations compared to small molecule inhibitors, which are often more potent, stable, have better pharmacokinetics, and are easier to produce (16, 17). However, to date, the development of small molecule fusion inhibitors against hCoVs has been remarkably limited, pointing toward the urgency of developing such molecules to treat SARS-CoV-2 and other related coronavirus infections.

Here, we used a rational drug repurposing approach to identify an FDA-approved small molecule that has the potential to interfere with the HR1–HR2 interaction and hence act as a broad-spectrum fusion inhibitor against different SARS-CoV-2 variants. First, we identified a novel, evolutionarily conserved "Ex_3Lx_6L" motif (abbreviated as E-L-L) in the HR2 domain of SARS-CoV-2 S and demonstrated that it plays a critical role in 6-HB formation and in fusion-mediated viral entry, thereby establishing it as a potential target for fusion inhibitors. Subsequently, *in-silico* screening led to the identification of posaconazole, a triazole antifungal drug (18), which we show, interacts with the "E-L-L" motif with high affinity. Posaconazole efficiently blocked HR1–HR2 complex formation in vitro and S protein-mediated cell-to-cell fusion in cultured cells, thereby establishing its fusion inhibitory potential. Our data show that posaconazole inhibits the entry of reporter viruses harboring SARS-CoV-2 S as their sole surface glycoprotein. Interestingly, mutations of the "E-L-L" residues make the S pseudotyped viruses resistant toward posaconazole, while mutations of adjacent residues show no such effect, confirming high specificity of the drug toward the "E-L-L" motif. Finally, we demonstrated the efficacy of posaconazole in inhibiting SARS-CoV-2 infection in Caco-2 cells through specific inhibition of membrane fusion, syncytium formation, and entry of viral genomic RNA into the host cells. Posaconazole also showed undiminished activity against the highly contagious Beta (B.1.351), Kappa (B.1.617.1) Delta (B.1.617.2), and Omicron (B.1.1.529) variants of SARS-CoV-2, thereby establishing itself as a new generation of small molecule fusion inhibitor against CoV infections.

Results

Identification of a highly conserved "E1182/L1186/L1193" motif in the HR2 domain of the SARS-CoV-2 S protein

To identify drug molecules that can destabilize the 6-HB structure, we attempted to find unique, highly conserved residues in the HR1 or HR2 domains of the SARS-CoV-2 S protein (Figure 1A), which are indispensable for 6-HB formation. For this, we analyzed the S protein sequences of all seven known human CoVs (hCoVs), including all reported variants of SARS-CoV-2, SARS-CoV, MERS-CoV, OC43, NL63, HKU1, and 229E. Sequence alignment between SARS-CoV-2 and SARS-CoV revealed high conservation in amino acid sequences for both HR1 and HR2 domains, which reduced significantly when compared with other β-hCoVs, MERS-CoV, OC43, and HKU1 and even more drastically when compared with α-hCoVs, NL63, and 229E (Figure S1A and B). Between all coronaviruses, the HR1 domain is more conserved with seven completely conserved residues compared to three completely conserved residues of the HR2 domain (Figure 1B). The three conserved residues in the HR2 correspond to E1182, L1186, and L1193 of SARS-CoV-2 S. The L1186 residue remains conserved across all CoVs except hCoV-HKU1, where it is replaced with a structurally homologous isoleucine residue (Figure 1B). In addition to all hCoVs, the identity of these three residues is retained across a wide variety of non-human CoVs (Figure 1C), suggesting that these residues remain conserved throughout the course of evolution of CoVs in a wide variety of host species and hence may serve an important role in the function of the S protein.

Structural analysis of the SARS-CoV-2 S 6-HB fusion-core revealed that the E1182, L1186, and L1193 residues in HR2 participate in either intrachain or interchain hydrophobic, hydrogen, and ionic interactions with the cognate groove formed by two adjacent HR1 helices (Table S1 and Figure 1D to F). The negatively charged carboxylate side chain of E1182 engages in electrostatic and/or hydrogen bonding interactions with suitably placed positively charged or donor moieties within the HR1 domain of the neighboring protomer (Figure 1F, upper panel and Table S1), while the neutral hydrocarbon side chains of L1186 and L1193 participate in multiple hydrophobic interactions with the HR1 domain of the same or neighboring spike protomers (Figure 1F, middle and lower panels and Table S1). The distance between the α-carbon atoms of E1182 and L1186 was found to be 6.3 Å, while the distance between L1186 and L1193 is 10.7 Å and the angle between the α-carbon atoms of E1182–L1186–L1193 is 150.2° (Figure 1G). Interestingly, the spatial organization of these three residues is completely conserved within the 6-HB structure of various other hCoVs (Figure 1G and H), which suggests that the "E-L-L" residues together constitute a highly conserved structural motif responsible for the stabilization of the 6-HB.

The "E-L-L" motif is critical for HR1–HR2 interaction and stability of the 6-HB structure

Molecular dynamic (MD) simulation experiments were performed to investigate the importance of the "E-L-L" motif in stabilizing the interaction between one pair of HR1–HR2 fusion-cores. Hundred nanoseconds (ns) simulation experiments were conducted using a pair of HR1–HR2 helices (residues 927 to 949 and 1,180 to 1,198, respectively; Protein Data Bank (PDB) ID: 6LXT) with either wild type (WT) or mutant HR2 peptides harboring single, double, or triple mutations as follows: E1182A, E1182K, L1193G, E1182K–L1186G, and E1182K–L1186G–L1193G. HR1–HR2 bis-peptide with single mutations in the HR2 domain showed structural stabilities, compactness, and mobility comparable to that of the WT as evidenced by the similar root mean square deviations (RMSD) (Figure 2A to C), radii of gyration (Rg) (Figure S2A to C), and root mean square fluctuation (RMSF) (Figure 2F and G) of the backbone atoms. In contrast, the double mutant E1182K–L1186G showed moderately high, while the triple mutant E1182K–L1186G–L1193G exhibited significantly higher RMSD (Figure 2D and E), Rg (Figure S2D and E), and RMSF values (Figure 2F and G), suggesting that the WT "E-L-L" motif is crucial for maintaining the structural integrity of the HR1–HR2 bis-peptide. It is worth noting that the small increase in the RMSD value of the E1182K (Figure 2A) mutant may indicate compromised backbone stability, due to the loss of the electrostatic/H-bonding interactions between the HR1 and HR2 peptides.

Estimation of the binding free energy of the WT and the different mutants by MM/GBSA method provided a more direct quantitative measurement of the interactions between these HR1 and HR2 peptides (Figure 2H). The WT bis-peptide is the most stable with ΔG value of −35.02 ± 3.83 kcal/mol, whereas E1182A and E1182K have ΔG values of −30.44 ± 2.32 kcal/mol and −33.96 ± 3.58 kcal/mol, respectively, suggesting that substitution of the glutamic acid at 1182 position exerted only marginal changes in the binding affinity between the HR1–HR2. Interestingly, the double mutant, E1182K–L1186G showed ΔG value of −24.06 ± 5.1, which is higher than that of the E1182K/A mutants, hence indicating that the L1186 residue is important for stabilization of the HR1–HR2 peptide complex structure. In addition, L1193 also plays a critical role in HR1–HR2 interaction as the L1193G mutant displayed ΔG value (−21.89 ± 3.43 kcal/mol) notably higher compared to other single mutants or the E1182K–L1186G double mutant. Finally, the triple mutant, E1182K–L1186G–L1193G, showed the highest free energy (−16.80 ± 3.01 kcal/mol) amongst all of the HR1–HR2 peptide complexes, reinstating the requirement of the complete "E-L-L" motif in stabilizing the HR1–HR2 interaction.

Next, we investigated the importance of the "E-L-L" motif in stabilizing the complete 6-HB structure constituted of the three pairs of the HR1–HR2 helices in the trimeric spike (PDB ID: 6LXT). MD simulation experiments were conducted for 100 ns with three pairs of HR1–HR2 helices harboring either WT (E-L-L) or mutant (K-G-G) motif in the HR2 helices. As observed from the RMSD (Figure S2F and G), the Rg (Figure S2H), and RMSF (Figure S2I to N) calculation of the backbone atoms, complete alteration of the "E-L-L" motif resulted in significant perturbation of the 6-HB structure. Together, these observations strongly indicate that the "E-L-L" motif is critical for stabilizing the HR1–HR2 interaction and hence for the formation of the 6-HB/fusion-core structure in the postfusion form of the S protein.

Mutations within the "E-L-L" motif impairs fusion-mediated entry of SARS-CoV-2 S pseudotyped lentiviruses in ACE2 expressing cells

Next, we evaluated the importance of the identified "E-L-L" motif in S-mediated viral entry processes. Reporter lentivirus harboring firefly luciferase gene in their genomic backbone and SARS-CoV-2 S protein as their surface glycoprotein has been reported to be a useful tool to study SARS-CoV2 entry in host cells (19). Hence, we have generated reporter viruses pseudotyped either with SARS-CoV-2 S or the vesicular stomatitis virus glycoprotein (VSV G) and used them to infect either HEK293T cells or HEK293T cells overexpressing ACE2 receptor. The efficiency of viral entry and infection was quantified by measuring the reporter activity at 18 h of post-infection (hpi). SARS-CoV-2 S pseudotyped reporter virus showed preferential entry into the HEK293T-ACE2 cells, while the VSV G pseudotyped virus showed no such preference (Figure 2I). Subsequently, SARS-CoV-2 S pseudotyped viruses harboring single (E1182K and L1193G), double (E1182K/L1193G), or triple (L1182K/L1186G/L1193G) mutations within the "E-L-L" motif were compared with WT S pseudotyped viruses for their ability to infect HEK293T-ACE2 cells (Figure 2J). Mutations either at E1182 or at L1193 caused 40% and 60% reduction in reporter activity, respectively, confirming the importance of these two residues in the optimum activity of the S protein. In addition, L1186 was also found to be crucial as pseudoviruses harboring E1182K/L1186G mutations showed a 65% decrease in reporter activity. Finally, replacing all three residues of the motif (E1182K/L1186G/L1193G) resulted in an 85% reduction in reporter activity (Figure 2J), confirming that complete integrity of the "E-L-L" motif is crucial for S-mediated entry of pseudoviruses in target cells. All the mutants were expressed and were proteolytically cleaved at the S1–S2 junction with efficiencies comparable to the WT S protein (Figure 2K).

Next, we investigated the importance of the "E-L-L" motif in spike-mediated membrane fusion. After synthesis, a fraction of the S protein reaches the cell surface and is embedded into the cell membrane where they trigger multinucleated syncytia formation between infected and uninfected cells (20). HEK293T cells were co-transfected with plasmids overexpressing SARS-CoV-2 S protein and eGFP (HEK293T-S + GFP), and subsequently were co-cultured with HEK293T-ACE2 cells for 24 h before fixing and imaging. Cells expressing WT S protein generated multinucleated green fluorescence protein (GFP) positive syncytia, while cells expressing the E1182K mutant showed moderate reduction and the E1193G and E1182K/L1186G mutants exhibited a severe reduction (Figure 2L and M and Figure S3) in syncytium formation. More significantly, cells expressing the triple mutant, E1182/L1186G/L1193G were completely defective in membrane fusion (Figure 2L and M and Figure S3). We also confirmed that all the S proteins were expressed on the cell surface at similar levels through surface immunostaining (Figure 2N), indicating that these mutations in the HR2 domain do not impede S protein processing and maturation. These data along with the MD simulation observations unambiguously establish that the "E-L-L" motif plays an indispensable role in S-mediated membrane fusion by stabilizing the HR1–HR2 interaction and 6-HB structure formation.

In silico screening for drugs targeting the highly conserved "E-L-L" motif

The high conservation of the "E-L-L" motif and its importance in fusion-mediated viral entry drove us to explore it as a poten-

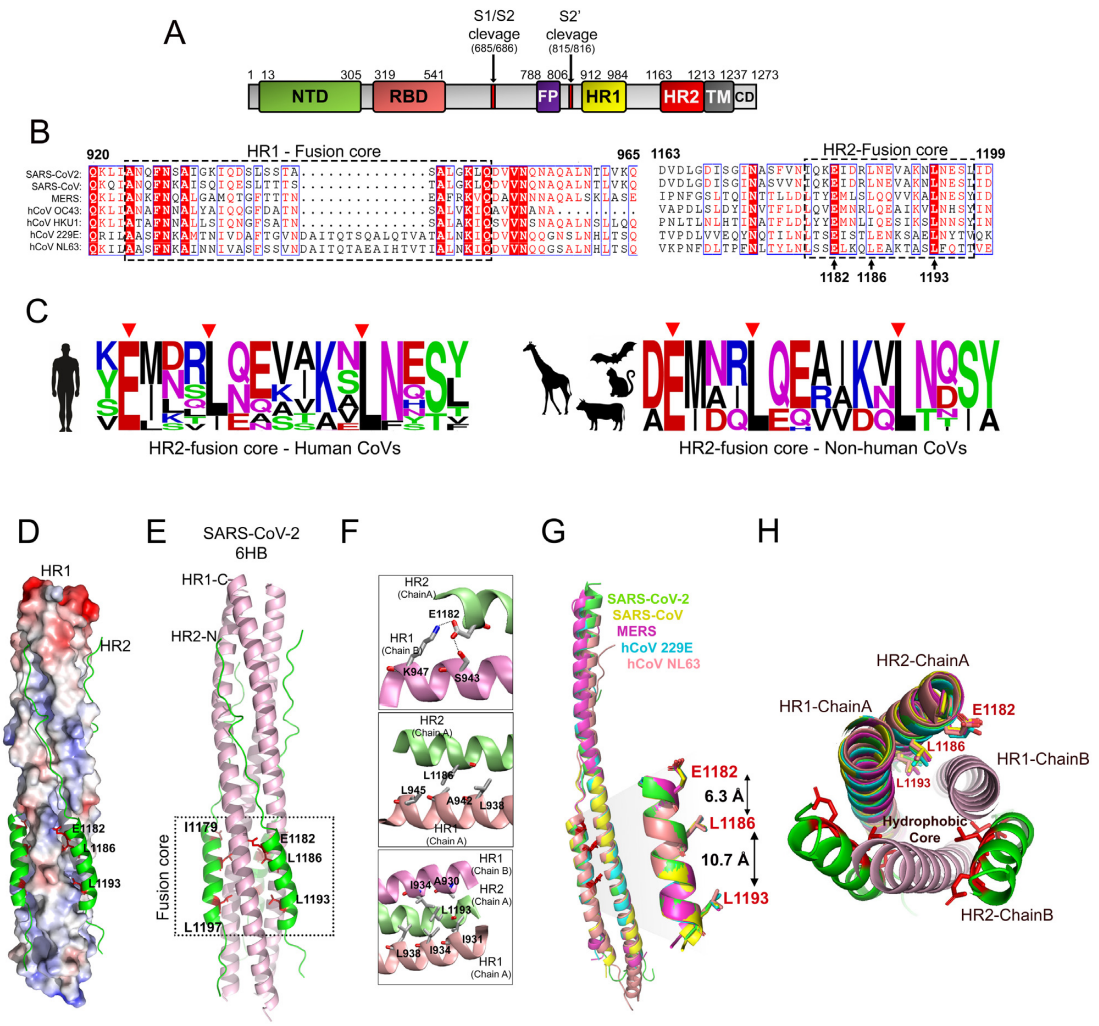

Fig. 1. An evolutionarily conserved "E-L-L" motif in the HR2 domain of SARS-CoV-2 S: (A) domain organization of SARS-CoV-2 spike protein. (B) Multiple sequence alignment of HR1 and HR2 domains of spike proteins from different human infecting coronaviruses with the fusion-core region highlighted by dashed rectangles. Amino acid residue numbers correspond to the SARS-CoV-2 S protein. (C) Logo plot representing amino acid frequencies in the fusion-core region of the HR2 from human or different animal infecting coronaviruses, highlighting the conserved E1182, L1186, and L1193 residues. (D) SARS-CoV-2 spike protein HR1 (surface charge representation) and HR2 (in ribbon representation) in the form of six-helix bundle (PDB ID: 6LXT). (E) Ribbon representation of three HR1 (light pink) and three HR2 (green) forming the 6-HB bracketed by the dashed rectangle. The E1182, L1186, and L1193 residues are highlighted in red stick representations. (F) Top. E1182 of HR2 from chain A (lime green) forming a salt bridge interaction and hydrogen bond with K947 and S943, respectively, of the HR1 of chain B (pink). Middle. Intramolecular hydrophobic interactions between L1186 of HR2 (chain A) and L-945, A-942, and L938 of HR1 (chain A, pale pink). Bottom. Intramolecular hydrophobic interactions between L1193 of HR2 Chain A and L938, I934, and I931 of HR1 chain A (pale pink), and A930 and I934 of HR1 chain B (pink). (G) Structural alignment of one pair of HR1–HR2 helices of different human infecting coronaviruses-green, SARS-CoV-2 (6LXT), yellow, SARS-CoV (1WYY), magenta, MERS-CoV (4NJL), cyan, 229E (5YL9), and pale orange, NL63 (2IEQ). The zoomed image represents the aligned HR2 fusion-core regions along with the side chains of the E1182, L1186, and L1193 residues. (H) Top view of the 6-HB structure of SARS-CoV-2 spike with one pair of the helix structurally aligned with that of the other coronaviruses as mentioned in G.

tial drug target for developing a broad-spectrum fusion inhibitor against coronaviruses. We mined standard chemical databases (PubChem, DrugBank Online, and Zinc15) and selected 25 potential candidates (22 FDA approved or under trial drugs and 3 previously reported small molecules, Figure 3 and Figure S4), that have stereo-electronic complementarity with the conserved "E-L-L" motif. We hypothesized that binding of the drug with the "E-L-L" motif would sterically hinder the association of HR1 and HR2 and therefore block the fusion process by destabilizing the 6-HB.

Molecular docking studies (21, 22) were carried out with a single pair of HR1–HR2 fusion-core helices as a receptor with the AutoDock grid (AutoDock 4.2) (23) set around the conserved "E-L-L" motif. To get more statistically accurate results, 500 docked conformations were generated for each of the 25 docked ligands, which were then grouped into different clusters (24). Each cluster contains one lowest energy seed conformation along with other structurally similar conformations (RMSD tolerance of 2.0 Å), all of which binds to a single pocket within the receptor. Thus, the number of conformations belonging to a specific cluster could be directly correlated with the probability of the ligand binding to a particular pocket. Using this analysis, we classified individual drugs based on three criteria: (i) lowest binding energy; (ii) number of conformations in the cluster containing lowest binding energy conformation; and (iii) ability of the drug to interact with the conserved "E-L-L" motif (Tables S2 and S3). Figure S5 represents a 3D plot for comparative analysis of the 25 drug molecules based upon all three criteria, while Figure 3A represents a 2D plot based upon the first two criteria. Posaconazole remained at the top of

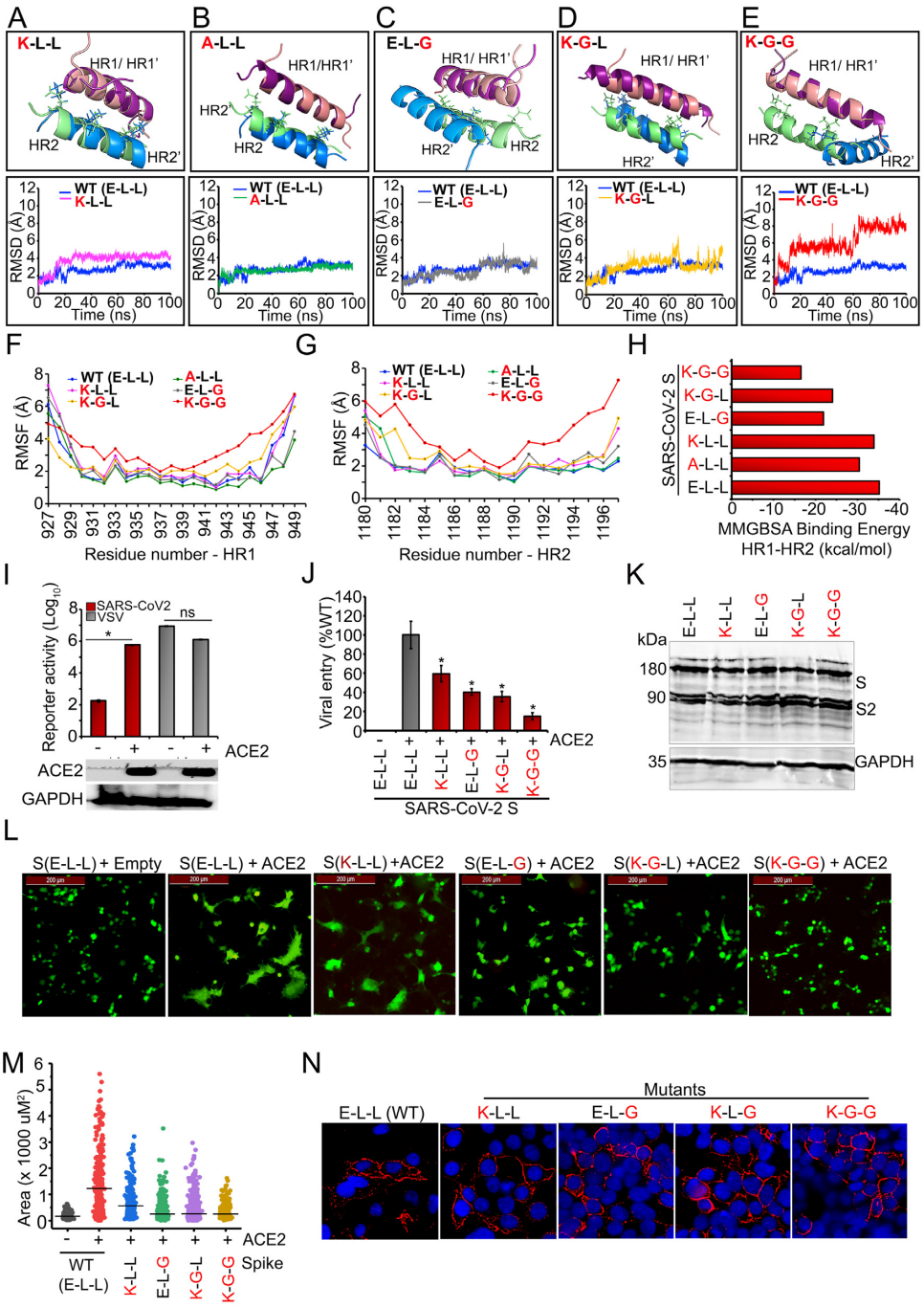

Fig. 2. The "E-L-L" motif is critical for 6-HB stability and fusion-mediated viral entry: (A–E) MD simulation experiments showing RMSD of the backbone atoms of HR1 and HR2 helices with the WT and mutant "E-L-L" motif. Upper panels represent one of the structural snapshots of the WT (HR1/HR2) and mutant (HR1'/HR2') bis-peptides during the simulation experiment. (F and G) RMSF analyses of the atoms present within the HR1 (F) and HR2 (G) helices in the context of WT or mutant bis-peptides. (H) Comparative assessment of MMGBSA binding energy for the WT and mutant dipeptides. (I) SARS-CoV-2 S or VSV G protein pseudotyped lentiviruses were used to infect either HEK293T or HEK293T-ACE2 cells. Luciferase activities were monitored as a measure of virus entry. (J) SARS-CoV-2 S protein (WT or mutants) pseudotyped viruses were tested for their ability to infect HEK293T-ACE2 cells. (K) WB analysis of the WT or mutant S proteins, expressed in HEK293T cells, using S specific antibody. (L) HEK293T overexpressing SARS-CoV-2 S (WT or mutants) and eGFP were co-cultured with HEK293T-ACE2 cells for 12 h and syncytium formation was monitored. (M) Area of the GFP positive cells was measured from ten independent fields to determine the mean syncytium area using ImageJ. (N) HEK293T cells were transfected with WT or mutant S protein-expressing plasmids and at 48 h post-transfection surface expression of the S proteins were evaluated using an anti-spike antibody.

the list in both of these analysis. Interaction profile of the HR1–HR2 helices with the drug molecules in their lowest binding energy conformation is represented in Figure 3B to D and H to J and Figures S6 and S7.

Posaconazole shows high affinity toward the "E-L-L" motif-containing binding pocket

To identify the drug with the highest potential of inhibiting the HR1–HR2 interaction, we focused on the top five drugs based upon

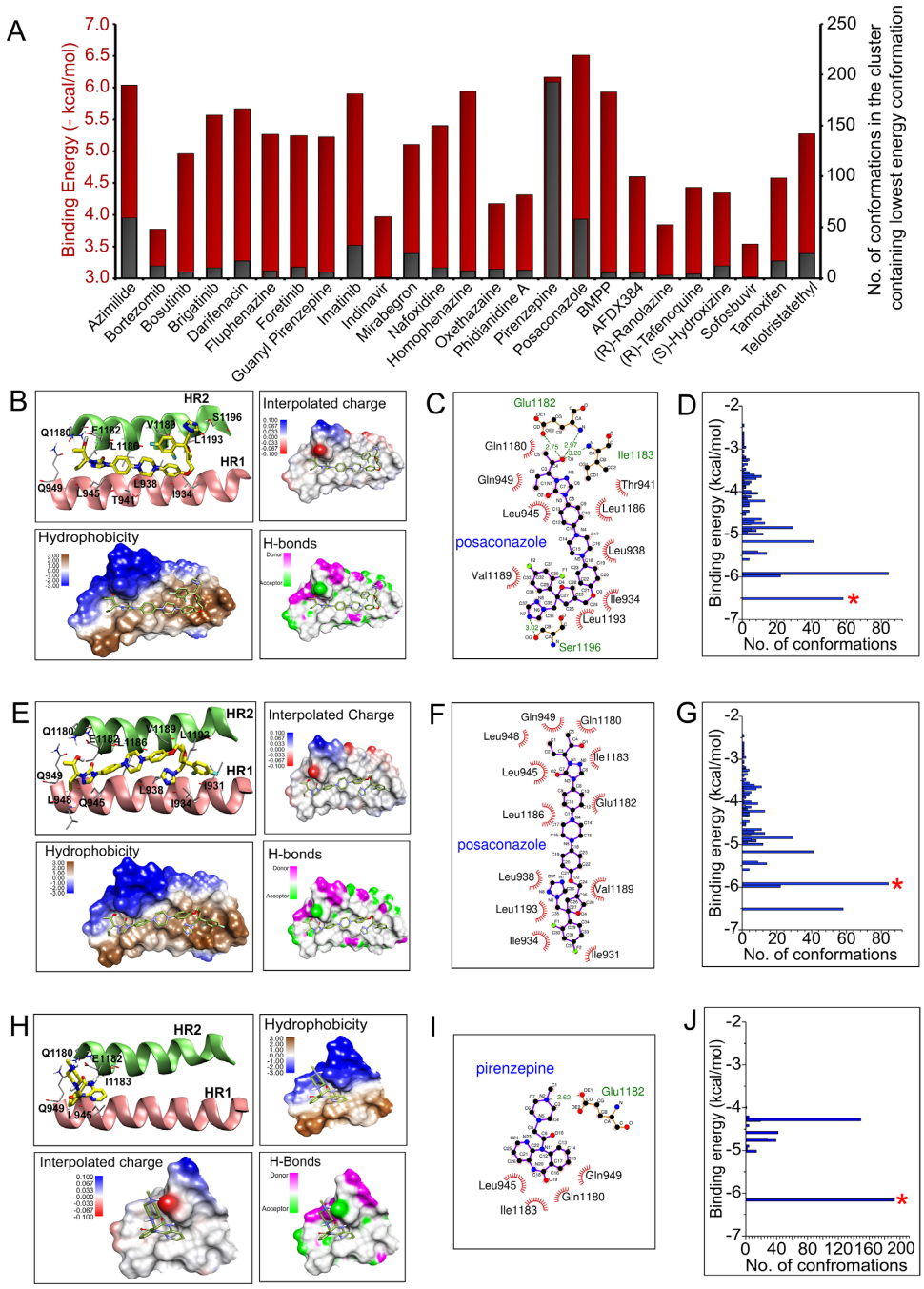

Fig. 3. In silico screening of drug molecules targeting "E-L-L" motif: (A) comparative plot of the lowest binding energies and number of conformations present in that cluster (containing the lowest binding energy conformation) corresponding to each of the docked molecules. Images (B) to (D) correspond to the lowest binding energy conformation of posaconazole; (E) to (G) corresponds to the lowest binding energy conformation from the most populated cluster for posaconazole; (H) to (J) correspond to the lowest binding energy conformation of pirenzepine. (B), (E), and (H) represent the binding pocket for each of the corresponding ligand conformation (HR1 and HR2 helix shown as cartoon image, ligand molecule, and the amino acid side chains shown in stick model); Hydrophobicity, hydrogen bond donor/acceptor, and interpolated charges on the protein surface for each corresponding ligand conformation have also been mapped. In (D), (G), and (J), the asterisk marks the particular cluster to which the corresponding ligand conformation belongs; (C), (F), and (I) are the ligplot images showing the corresponding ligand–protein interaction in 2D.

their binding energy—(i) posaconazole, (ii) pirenzepine, (iii) azimilide, (iv) homophenazine, and (v) BMPP (Figure 3A and Table S2), and analyzed their interaction profile with the "E-L-L" motif. Posaconazole (Figure 3B to D) and BMPP (Figure S6I to L), in their lowest binding energy conformation, interacted with the largest number of residues (Tables S2 and S4), including all three residues of the "E-L-L" motif. In contrast, azimilide and homophenazine interacted with fewer residues, including E1182 and L1186 (Figure S6A to H), while pirenzepine interacted selectively with E1182 along with a few more surrounding residues (Figure 3H to J). It is important to note that, posaconazole showed similar interaction profiles with HR1–HR2 both in their highest populated cluster and in the cluster containing lowest binding energy conformation (Figure 3B to G). In contrast, for pirenzepine, the cluster containing the lowest binding energy conformation remained highest populated (Figure 3H to J) (see footnote in Supplementary Material

Appendix). Based on these analyses, we focused our attention on posaconazole and pirenzepine for further investigation.

Posaconazole inhibits SARS-CoV-2 S pseudotyped lentivirus entry, specifically targeting the "E-L-L" motif

Having determined posaconazole and pirenzepine to be the two most suitable candidates, we tested the ability of these two drugs in blocking SARS-CoV-2 S pseudotyped lentivirus entry into ACE2 expressing cells. SARS-CoV-2 S pseudotyped lentiviruses were pretreated with increasing concentrations of either posaconazole or pirenzepine before infecting HEK293T-ACE2 cells, which were then further incubated in the respective drug concentration until harvest. Treatment with posaconazole resulted in a dose-dependent decrease in SARS-CoV-2 pseudovirus entry with more than 90% reduction in reporter gene expression at a concentration of 10 μM (Figure 4A), whereas pirenzepine did not have any significant effect (Figure 4B). The half effective inhibitory concentration (IC_{50}) of posaconazole was estimated to be 3.37 μM (Figure 4C). However, posaconazole did not inhibit the entry of control VSV G pseudotyped viruses (Figure 4A), suggesting that the drug specifically blocks SARS-CoV-2 entry. We also showed that posaconazole does not have any significant inhibition toward the entry and infection caused by two other enveloped viruses, influenza A/H1N1 (Figure 4D) and herpes simplex virus 1 (HSV1) (Figure 4E), hence establishing its specificity in blocking the entry of SARS-CoV-2. Interestingly, pirenzepine, although showed similar binding affinity (6.16 kcal/mol) to posaconazole (6.51 kcal/mol) in silico, failed to impact entry of SARS-CoV-2 S (Figure 4B), possibly because it specifically interacts only with residue E1182 and not with the whole "E-L-L" motif. Both these drugs were nontoxic at the concentrations used (Figure S8).

To unambiguously establish the selectivity of posaconazole toward the "E-L-L" motif, we tested its efficacy against viruses pseudotyped with the SARS-CoV-2 S protein harboring mutations within the "E-L-L" motif. Pseudoviruses harboring single S mutations, E1182K and L1193G, showed almost similar sensitivity compared to the WT (Figure 4F). In contrast, pseudoviruses harboring double or triple mutation within the "E-L-L" motif became highly resistant toward Posaconazole (Figure 4F). Clearly, substituting two of the three residues of the "E-L-L" motif makes the SARS-CoV-2 S protein completely resistant toward the drug, establishing the high selectivity of posaconazole toward this motif. To further substantiate this phenomenon, we carefully looked into the HR2 fusion core sequences (Figure 1B and C) to identify amino acid residues, which are in between the E-L-L residues but are not a part of the motif. We have selected arginine 1185 and asparagine 1192 as these two residues are conserved across all available sequences of SARS-CoV2 S protein. However, structurally these residues are projected toward the opposite face of the HR2 helix in comparison to the residues constituting the "E-L-L" motif (Figure 4G), hence should not directly interact with Posaconazole. To test this, we have generated pseudoviruses harboring either R1185A or R1185A/N1192A mutations and tested their entry efficiency. As shown, mutation of the R1185 residue shows no impact, while mutation of both R1185 and N1192 residues showed ~50% reduction in comparison to the WT pseudovirus entry (Figure 4H). Interestingly, both of these mutant pseudoviruses retained sensitivity toward posaconazole, as pretreatment with the drug resulted in ~50% to 60% reduction in their entry (Figure 4I). This data suggest that residues surrounding the "E-L-L" motif may play a role in mediating fusion by either directly participating in interactions with the HR1 helix or by helping to maintain the overall structural integrity of the HR2 helix. However, posaconazole specifically targets the "E-L-L" residues to interact with HR2 and interfere with the formation of the 6-HB complex.

Posaconazole inhibits HR1–HR2 interaction and subsequent syncytium formation

We next investigated the molecular mechanism by which posaconazole blocks the cellular entry of S protein pseudotyped viruses. For this, we recombinantly overexpressed and purified the HR1 and HR2 domains from *Escherichia coli* and reconstituted the 6-HB complex in vitro. As shown in Figure 5A, when increasing concentrations of HR1 and HR2 proteins were mixed and incubated for 30 min, they formed a slow migrating, higher molecular weight complex in native-PAGE. In contrast, the HR2 protein harboring triple mutation at the "E-L-L" motif (K-G-G) failed to reconstitute the high molecular weight complex with HR1, substantiating the importance of this motif in forming the 6-HB (Figure 5A). In addition, when incubated in the presence of increasing concentration of posaconazole, we observed a gradual decrease in intensity of the HR1–HR2 complex in native-PAGE (Figure 5B), which confirms that this drug can directly interfere with the 6-HB formation.

Posaconazole blocks 6-HB formation, which is a prerequisite for membrane fusion. Hence, we tested the ability of posaconazole to inhibit membrane fusion by syncytia formation assay. Pretreatment of HEK293T-S + GFP cells with increasing concentrations of posaconazole and their subsequent co-culturing with HEK293T-ACE2 cells resulted in significant reduction in syncytium formation in comparison to the control set (Figure 5C and D and Figure S9). Together, the data presented so far establish that posaconazole specifically inhibits SARS-CoV-2 S-mediated entry, by blocking the fusion of viral and host membranes, specifically targeting the highly conserved "E-L-L" motif present in the HR2 domain of the S protein.

Posaconazole efficiently inhibits S-mediated entry of newer SARS-CoV-2 variants of concern (VoC)

Of late, the Delta (B.1.617.2) and Kappa (B.1.617.1) variants of SARS-CoV-2 have been a matter of immense concern (3, 25). The Delta variant has been declared as one of the main VoC associated with higher infectivity, hospitalization, reinfection, and infection in vaccinated individuals (26). More recently, the Omicron (B.1.1.529) VoC was identified with a staggering 30 mutations in its S gene and has been predicted to have even higher infectivity than the Delta variant (27). Interestingly, the "E-L-L" motif and all of the residues across HR2 and HR1 helices that participate in interaction with posaconazole are highly conserved across all different variants, including the Delta, Kappa, and Omicron VoCs (Figure 6A and Figure S10), suggesting that posaconazole should be effective against these more virulent variants of SARS-CoV-2. Posaconazole exhibited strong inhibitory effects on the entry of the pseudoviruses harboring S protein from D614G variant, the dominant clade of SARS-CoV-2 (28), the Kappa (B.1.617.1), Delta (B.1.617.2), and the Omicron (B.1.1.529) variants, which are comparable to that of the original Wuhan strain (Genbank NC_045,512) (Figure 6B), hence confirming its efficacy against newer and deadlier variants of SARS-CoV-2.

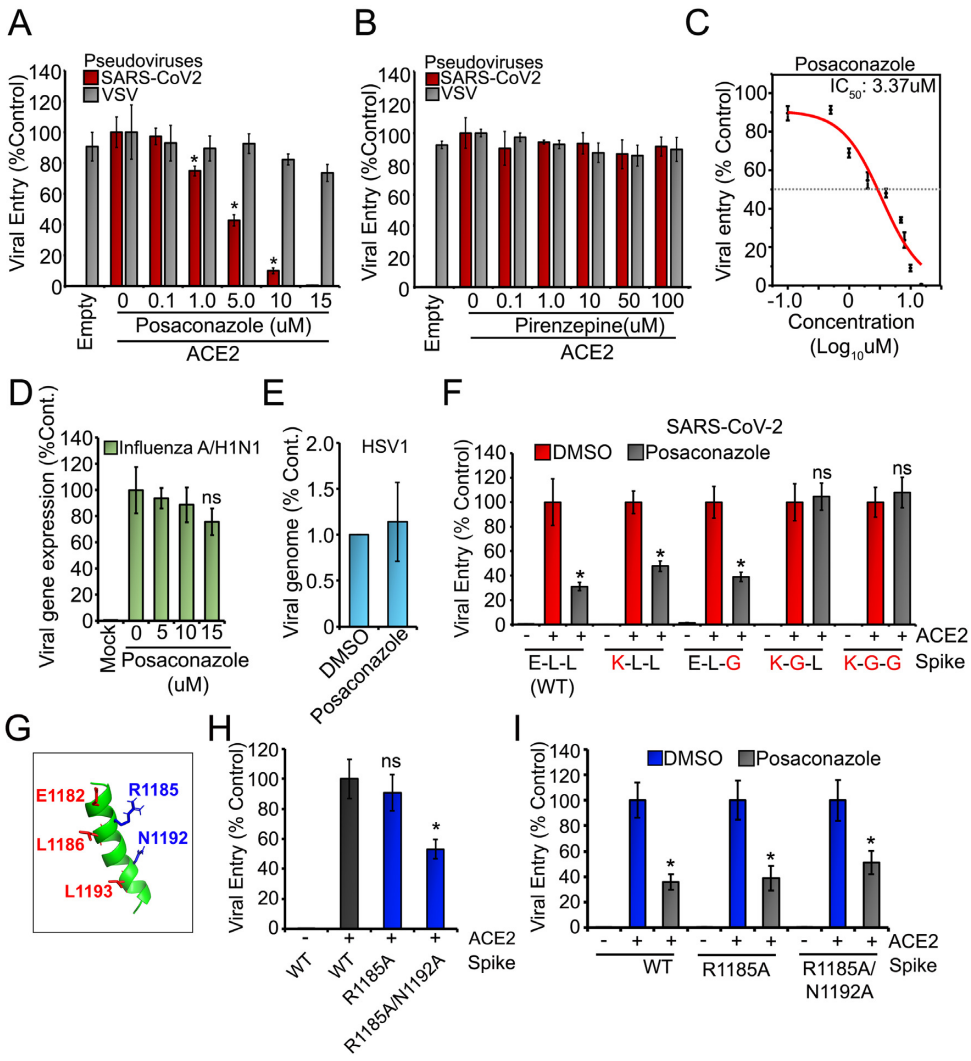

Fig. 4. Posaconazole inhibits SARS-CoV-2 S pseudotyped lentivirus entry by targeting the "E-L-L" motif. (A) and (B) SARS-CoV-2 S or VSV G pseudotyped reporter viruses and were pretreated with Dimethyl sulfoxide (DMSO) or with different concentrations of the indicated drugs and used to infect either HEK293T (empty) or HEK293T-ACE2 cells in presence of the drug. Reporter activity was measured at 18 h and plotted as a relative percentage to the DMSO treated sets. (C) IC_{50} of posaconazole against the SARS-CoV-2 S pseudotyped viruses was calculated by fitting reporter assay data in the four-parameter nonlinear equation in origin lab software. (D) Madin-Darby canine kidney (MDCK) cells were infected with the influenza A (WSN/H1N1/1933) nano-Luc reporter virus pretreated with DMSO or with different concentrations of posaconazole and reporter activity was measured at 8 hpi. (E) Vero cells were infected with HSV1 pretreated with DMSO or with 8 μM posaconazole and viral genome was quantified at 2 hpi using qPCR. (F) WT or mutant SARS-CoV-2 S pseudoviruses were treated with posaconazole before, during, and after infecting HEK293T-ACE2 cells with them. Reporter activity was measured and plotted as a relative percentage of the DMSO treatment for each set (WT and mutant viruses). (G) Spatial organization of the residues constituting the E-L-L motif (E1182, L1186, and L1193) and two other residues in between (R1185 and N1192). (H) HEK293T-ACE2 cells were infected with pseudoviruses harboring WT or mutant (R1185A/N1192A) spike proteins to check their entry efficiency. (I) WT or mutant (R1185A/N1192A) pseudoviruses were treated with posaconazole before, during, and after infecting HEK293T-ACE2 cells with them. Reporter activity was measured and plotted as a relative percentage of the DMSO treatment for each set (WT and mutant viruses).

Posaconazole inhibits SARS-CoV-2 infection through blocking S-mediated membrane fusion and subsequent release of viral genomic RNA in Caco-2 cells

Next, we tested the efficacy of posaconazole as a fusion inhibitor on infectious SARS-CoV-2 virus. Using a fluorescently labeled recombinant virus based on the 2019-nCoV/USA-WA1/2020 strain, SARS-CoV-2-mNG (29), we evaluated three different concentrations of the drug, for anti-SARS-CoV-2 activity. Caco-2 cells, pretreated with the respective concentrations of posaconazole were infected with SARS-CoV-2-mNG, also pretreated with the corresponding concentrations of the drug. At 48 hpi, we observed a dose-dependent decrease in mNG signal (Figure 7A and B and Figure S11) indicating efficient inhibition of SARS-CoV-2 infection. We followed up this experiment with a plaque assay under similar conditions but using nonrecombinant WT SARS-CoV-2 and observed greater than 1 log reduction of virus titer at all three concentrations tested with 8 and 12 μM showing the greatest but similar inhibition of the virus (Figure 7C and Figure S12A). Posaconazole was nontoxic at these concentrations, and we selected 8 μM for all downstream experiments. Posaconazole also inhibited the infection of more recent variants of SARS-CoV-2, including the Beta variant (also known as South African variant) and the Delta variant at efficiencies equal to the WT variant (Figure 7D and Figure S12B). Furthermore, we evaluated the fusion inhibition potential of posaconazole on SARS-CoV-2-mNG infected

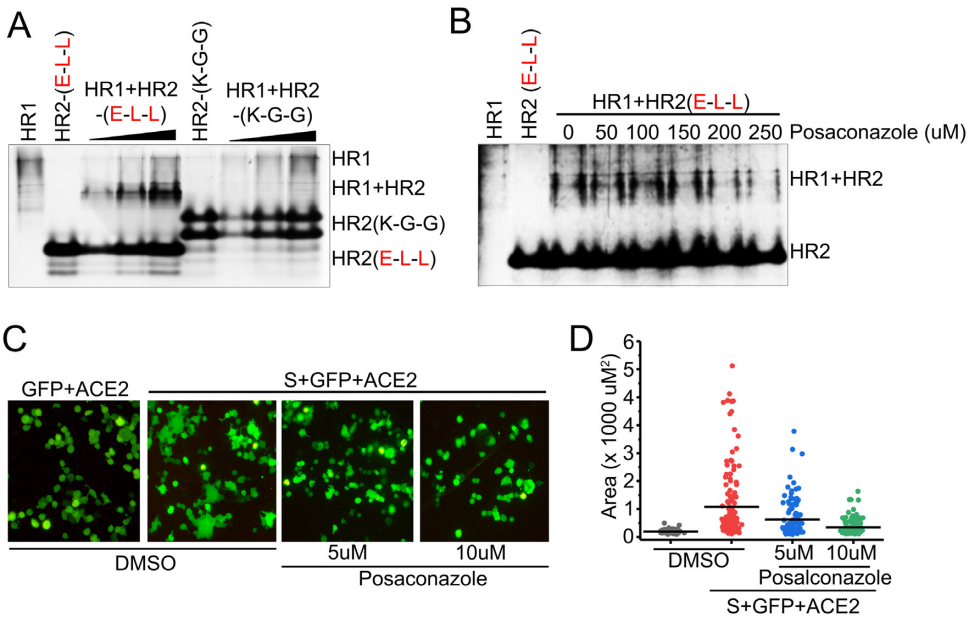

Fig. 5. Posaconazole inhibits HR1–HR2 complex formation and cell-to-cell fusion. (A) Purified HR2 protein either harboring WT "E-L-L" or mutant "K-G-G" motif were incubated with purified HR1 protein in increasing concentrations to form the 6-HB complex, which was then analyzed using native PAGE. (B) HR2 (WT) and HR1 proteins (25 μM each) were incubated either in the absence or in the presence of increasing concentrations of posaconazole followed by which HR1–HR2 complex formation was analyzed through native PAGE. (C) Cells expressing SARS-CoV-2 S and GFP were treated with different concentrations of posaconazole or with DMSO before and during co-culturing them with HEK293T-ACE2 cells for syncytium formation assay. (D) The area of the GFP positive cells was measured from five independent fields and the mean area plotted using ImageJ software.

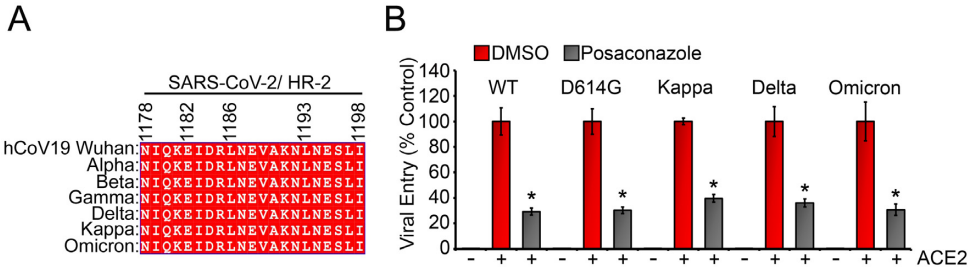

Fig. 6. Posaconazole inhibits entry of SARS-CoV2 variants. (A) (I) Amino acid alignment of the posaconazole interacting region of HR2 from major VoC as obtained from the GISAID database. (B) HEK293T-ACE2 cells were infected with pseudoviruses expressing S proteins of either WT SARS-CoV-2 (Wuhan strain) or major VoC's (D614G, Delta, Kappa, and Omicron), treated with DMSO or with posaconazole before, during, and after infection. Reporter activity was plotted as a relative percentage to the DMSO control for each set. $* = P < 0.001$ (unpaired Student's *t*-test). Images shown are representative of three independent repeats.

Caco-2 cells by visualizing and measuring the syncytia formed after 48 hpi (Figure 7E and F and Figure S13). As evident, posaconazole treatment drastically reduced syncytium size confirming that it inhibits membrane fusion between adjacent cells.

As successful fusion of viral and host cell membranes leads to the release of the viral genome into the host cell, we evaluated the effect of posaconazole upon the accumulation of SARS-CoV-2 genomic RNA at different time points post-infection. Cells were infected with SARS-CoV-2 with or without posaconazole treatment and qRT-PCR was performed to quantify the amount of viral genomic RNA at different time points post-infection. When normalized to its corresponding mock treatment, posaconazole resulted in a gradual decrease in viral RNA abundance with time (Figure 7G) with more than 95% reduction at 48 hpi. Interestingly, at 2 to 12 hpi, we observed a 64% reduction in the abundance of viral RNA, indicating that posaconazole inhibited the initial infection of the virus (2 hpi) as well as subsequent rounds of progeny virus release and infection of neighboring cells (24 and 48 hpi). When normalized to the initial inoculum of viral RNA (2 hpi), the DMSO treated cells exhibited an exponential increase in viral RNA up to about 30 hpi, where after, it plateaued (Figure 7H). Posaconazole treated cells under similar conditions exhibited greatly reduced virus replication kinetics confirming its robust antiviral potential (Figure 5H). We also confirmed that posaconazole neither affected the migration of S protein to the cell membrane (Figure 7I and Figure S14), nor did it affect S protein synthesis and/or stability (Figure 7J).

Finally, we performed time of treatment assays to study the efficacy and mechanism of action of posaconazole. As illustrated in Figure 8A, for a prophylactic setting, viruses and the cells were (a) preincubated with posaconazole for 1 h, which were then used for infection in absence of the drug, or (b) treated during the infection followed by washing off the drug. We also included sets where cells were treated with posaconazole (c) only post-infection, or (d) both during and after infection. In another set (e), both the virus and cells were treated with posaconazole at "all times," pre, post,

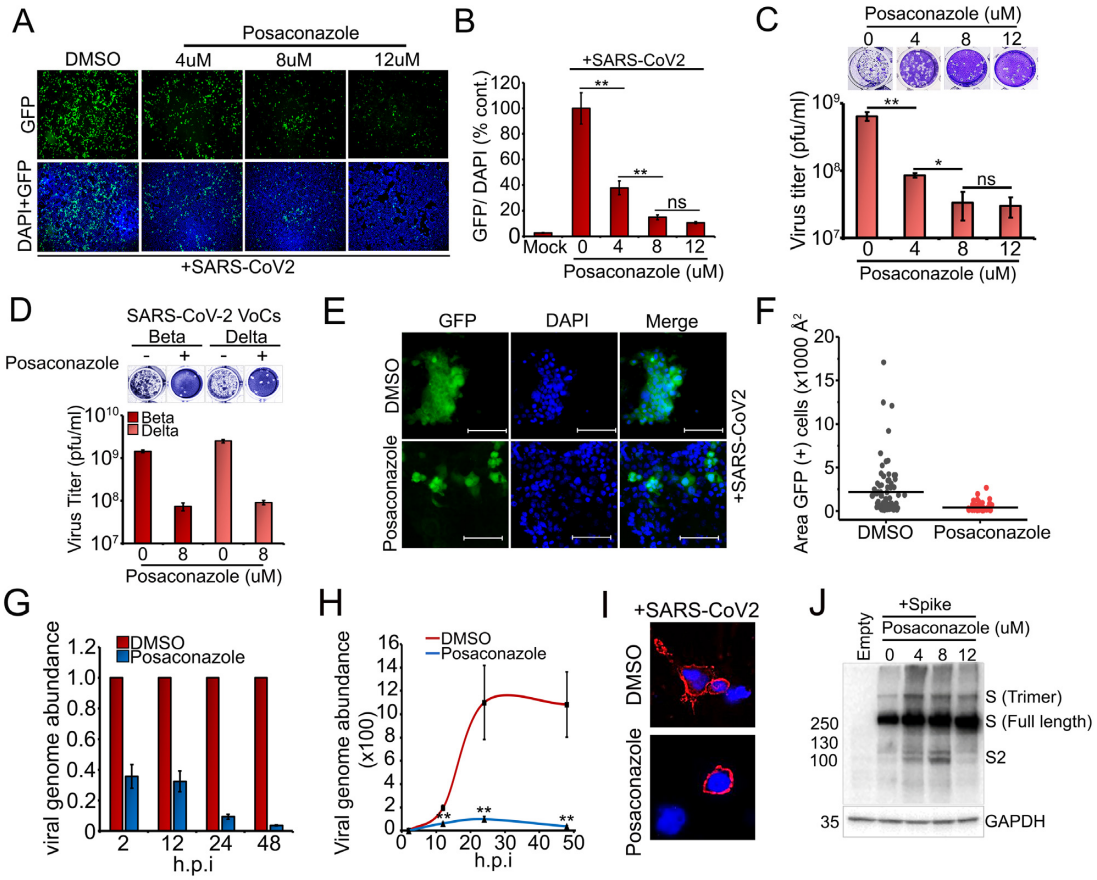

Fig. 7. Inhibitory effects of posaconazole on infectious SARS-CoV-2 virus. (A) Caco-2 cells pretreated for 1 h with DMSO or the indicated concentrations of posaconazole were infected with SARS-CoV-2-mNG virus (multiplicity of infection, MOI of 0.1) also pretreated with corresponding concentrations of the drug. At 48 hpi, mNG fluoresence was visualized and quantitated using ImageJ (B). mNG signals were normalized against DAPI signals and plotted relative to DMSO treated samples. (C) and (D) Caco-2 cells were infected either with WT SARS-CoV-2 (C) or with the Beta or Delta variants (D) pretreated with DMSO or posaconazole (8 μM) and after 48 hpi, the infected supernatants were titrated using plaque assay. (E) Caco-2 cells, pretreated with posaconazole (8 μM), were infected with pretreated SARS-CoV-2-mNG (MOI 0.1) and visualized at 40X for syncytia formation. (F) The area of each syncytium was measured using ImageJ and plotted. (G) Caco-2 cells pretreated with DMSO or posaconazole (8 μM) and were infected with pretreated SARS-CoV-2. Total RNA extracted at indicated times, were evaluated by qRT-PCR. The data are expressed as fold changes of the viral N RNA levels normalized to RNaseP control relative to the corresponding DMSO treated samples. (H) Similar experiment as in (G), but expressed as relative to the initial inoculation amount (at 2 hpi). (I) Surface immunofluorescence assay for the S protein was performed on Caco-2 cells infected with WT SARS-CoV-2 in presence of DMSO or posaconazole (8 μM). (J) WB of the S protein 72 h after infection of Caco-2 cells with WT SARS-CoV-2 in the presence of DMSO or different concentrations of posaconazole.

and during infection. As observed (Figure 8B and C and Figure S15), post-treatment of the drug alone had a much-diminished effect on reducing infection compared to the other time of addition experiments. Moreover, treatment only during infection had an almost similar outcome as the "all-time" treated sets. Both pre + during and during + post treatments had comparable inhibitions to the "all-time" treated samples. This confirms that posaconazole functions as a fusion inhibitor and its presence during infection is enough to exhibit a robust antiviral effect. Additionally, post-infection treatment of the cells with posaconazole also showed a significant effect, possibly rooted through its effect on blocking subsequent rounds of infection of neighboring cells. Together, these data confirm that posaconazole act as a fusion inhibitor that can inhibit SARS-CoV-2 at the entry stage of infection and also suggest that it has both, prophylactic, as well as, therapeutic potentials.

Discussion

The rapid evolution of the SARS-CoV-2 resulting in recurrent surges of infection by different VoCs and its concomitant effect on global health and economy (3) calls for the development of novel therapeutic strategies, which will be able to combat both, the current and future variants. In this report, we describe the identification of a novel drug target in the viral spike glycoprotein and its subsequent targeting using a safe, pharmacologically approved molecule to develop an effective entry inhibitor against SARS-CoV-2.

Fusion inhibitors are of great potential to block the entry of enveloped viruses, which require fusion of the viral and host cell membranes to release their genetic material into the cytoplasm. Diverse families of viruses, including *Retroviridae*, *Orthomyxoviridae*, *Paramyxoviridae*, *Filoviridae*, and *Coronaviridae*, possessing Class I fusion proteins, share common structural mechanism for triggering membrane fusion. Interaction between three HR1 and HR2 domains of the trimeric fusion protein, leads to the formation of the 6-HB, which is critical for bringing the viral and host membranes in close proximity, hence driving their fusion (6, 8, 30–32). This makes the 6-HB structure an attractive drug target for blocking membrane fusion and viral entry (11–15, 33–38). However, till date, the 6-HB structure has been mostly targeted using long peptides (35 to 50 amino acids) mimicking either HR1 or HR2

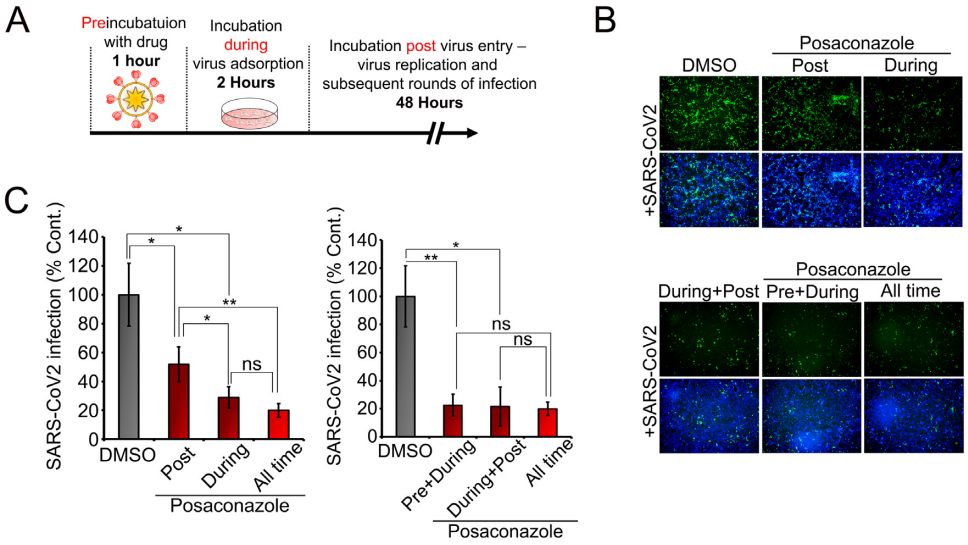

Fig. 8. Posaconazole blocks SARS-CoV-2 infection at early stage. (A) Schematic representation of the time of addition assay for posaconazole (8 μM) on Caco-2 cells infected with SARS-CoV-2-mNG (MOI 0.1). (B) and (C) mNG was visualized and quantitated by counting the mNG positive cells and normalized to the total DAPI signal in that field. All data shown are averages of the results of at least three independent experiments ± SD. * = $P < 0.05$; ** = $P < 0.01$; *** = $P < 0.001$, **** = $P < 0.0001$ (unpaired Student's *t*-test). Images shown are representative of all independent repeats.

helices (11, 13, 39–41). While these peptides show high efficacy in inhibiting virus replication, their widespread implementation as antiviral drugs will be challenging owing to the inherent limitations of peptide-based therapeutics (16, 17). On the other hand, bioavailable small molecule fusion inhibitors, which are both easier to produce and deliver than peptides, have been disappointingly scarce and only a handful have been described for IAV and HIV (35, 42) and more recently against CoVs (36, 43, 44).

Successful targeting of viral infection with small molecules requires identification of a suitable "molecular target" possessing the following characteristics: (i) it should represent a structural element or a sequential motif or a combination of both, which would offer a suitable interaction interface for the small molecule; (ii) the target region should be critical for the activity of the viral protein, and (iii) it should be minimally tolerant toward evolutionary changes acquired through antigenic drifts or shifts. Considering these parameters, in this study, we identified a highly conserved motif, E1182–L1186–L1193 present within the HR2 helix of SARS-CoV-2 S protein, whose side chains participate in essential molecular interactions indispensable for the stability of the 6-HB (Figure 1B, C, E, and F). MD simulation analysis suggested that mutation of these residues perturb the HR1–HR2 interaction and thus, alter the overall stability of the 6-HB fusion-core structure (Figure 2A to H). This was supported by our mutational analysis, which showed that alteration of either single or multiple amino acids of the "E-L-L" motif makes the S protein attenuated toward fusion and entry of SARS-CoV-2 S pseudotyped viruses in ACE2 overexpressing cells (Figure 2J, L, and M), while mutation of amino acids in between the "E-L-L" motif showed negligible effect (Figure 4H). Together, these data confirmed the importance of the "E-L-L" motif in the structure and activity of the S protein and established it as a novel molecular target for the discovery of a new generation of fusion inhibitors against CoVs.

We undertook a multidimensional in silico screening strategy to identify potential FDA-approved or under trial drugs capable of targeting this "E-L-L" motif. For this, we classified the drugs based on their binding energy toward the "E-L-L" motif, the number of conformations that are closely related to the lowest binding energy conformation and their potential to interact with amino acids constituting the motif. Posaconazole, emerged as the best candidate with significantly high binding affinities in two of the highest populated clusters and numerous molecular interactions spanning across the entire "E-L-L" motif. While posaconazole shows strong fusion inhibitory activity against the WT SARS-CoV-2 S protein (Figure 4A), mutation of more than one residues of the "E-L-L" motif makes the protein completely resistance toward the same (Figure 4F). Multiple mutations introduced in between the "E-L-L" residues show no impact upon posaconazole sensitivity (Figure 4I), substantiating the high specificity of the drug toward this motif. Though the appearance of such drug resistant mutations might seem to be of concern for possible appearance of posaconazole-resistant variants, the high conservation of the "E-L-L" motif across all reported variants of SARS-CoV-2 and amongst other CoVs point toward the high genetic/evolutionary barriers that these viruses have to overcome in order to develop such resistance. In fact, the mutant "K-G-G" HR2 peptide is completely defective in forming the HR1–HR2 complex in vitro (Figure 5B), suggesting that the SARS-CoVs are least tolerant toward alterations in the "E-L-L" motif, establishing it as an ideal target for broad-spectrum fusion inhibitors.

Posaconazole is an azole antifungal drug approved by the US FDA in 2006 (18). In our studies, it exhibited high efficacy in inhibiting entry and replication of SARS-CoV-2 and its VoCs. Syncytia formation in infected lungs cells has been recognized as a hallmark of severe stages of SARS-CoV-2 infection with strong implications in the pathogenic outcome of the patient (45). Our data confirmed that posaconazole specifically inhibits HR1–HR2 complex formation in vitro, which serves the basis for its activity in blocking S-mediated membrane fusion, syncytium formation, and subsequent release of viral genome in host cells. Posaconazole blocks the virus at early stages of infection, making it superior to the currently available drugs that target RdRp activity and hence block the later stages of infection (46). Therefore, an exciting proposition toward a novel anti-SARS-CoV-2 therapy can be the use of posaconazole as a prophylactic nasal spray to inhibit early colonization of the virus in the upper respiratory tract and subse-

quent administration of oral suspension of the drug as a therapeutic to prevent or treat lower respiratory tract infection. The pharmacokinetics of posaconazole is well studied where a recommended 400 mg twice daily dosage results in mean peak drug plasma concentrations (C_{max}) of 4.15 μg/ml, or 6 μM (47), which is comparable to the effective cell-culture concentration of the drug we observed in our studies. Posaconazole showed a favorable safety profile, with only ⩽2% of patients exhibiting side effects when administered in a dose of 400 mg/day for 24 weeks (48). Most interestingly, posaconazole is under clinical trial for treating COVID19 associated pulmonary aspergillosis (49, 50), hence establishing it as a safe option to treat both SARS-CoV-2 and associated secondary fungal infections. Recent *in-silico* analysis also point toward posaconazole's role as a SARS-CoV-2 helicase inhibitor (51), which is however yet to be experimentally validated.

Together, our study provides the mechanism and rationale for repurposing posaconazole as a potential anti-SARS-CoV-2 drug. Easy and ready availability, low toxicity, and well-known pharmacokinetics of posaconazole along with its proven efficacy against different variants of SARS-CoV-2 will support initiation of fast-track clinical trials for rapid dissemination of the drug as the next generation antiviral therapy to treat COVID19 disease.

Materials and methods

Bioinformatics and structural analysis

Amino acid sequences of different human infecting CoV spike proteins were obtained from NCBI database. HR1 and HR2 regions of the specific proteins were aligned using clustalW multiple sequence alignment function (MSA) in Bioedit. Representative image was generated using ESPript 3.0. MSA data were used to calculate amino acid identity matrix for HR1 and HR2 regions. Conservation of E-L-L motif was checked by searching "E-L-L" sequence in different human/animal coronavirus HR2 regions. Identified regions are aligned and logoplots were generated using WebLogo (https://weblogo.berkeley.edu/logo.cgi). Structural alignment was performed in Pymol. Protein–protein interactions were calculated using PIC webserver (http://pic.mbu.iisc.ernet.in/).

MD simulations

All the peptide-chains were subjected to 100 ns MD simulations in explicit solvents (Supplementary Material). Helix-bundles, WT and mutated, both contained three chains A, B, and C from the PDB entry 6LXT. Steepest descent algorithm was used to energy minimize the solvated protein structures with maximum force limit of 1000 kJ/mol/nm. For equilibration, 100 ps simulations were carried out using NVT (canonical ensemble) and NPT (isothermal-isobaric ensemble)ensembles at temperature 300 K and pressure 1 bar, respectively. MMGBSA analyses were carried out using 200 snapshots from the last 10 ns of the MD simulations.

Screening of small molecules; molecular docking

3D structures of the ligands were made using Chem 3D Pro or procured from databases like PubChem, Drugbank online, etc. Docking was performed with Autodock4.2 employing Lamarckian Genetic Algorithm to find the best docked pose. The docked complexes were visualized using MGL Tools-1.5.6, Discovery Studio 2019 Client, and VMD. The 2D-interactions were interpreted from the image obtained through LigPlot v2.2.4.

Assessing the effect of drugs upon SARS-CoV-2 S and VSV-G pseudotyped lentivirus entry

Lentivirus particles pseudotyped with WT and mutant (for primers sequences see Table S5) SARS-CoV-2 S protein were generated following Katharine et al. (19) and described in detail in Supplementary Material Appendix. Reporter lentiviruses pseudotyped with either SARS-CoV-2 S (WT or different variants or mutants) or VSV-G were treated with different concentrations of drugs for 30 min at RT. HEK 293T or HEK293T overexpressing ACE2 cells were infected with treated viral inoculum for 1 h at 37°C in presence of the drug and subsequently replenished with fresh media with the same concentration of the drugs. Infected cells were harvested at 18 hpi and luciferase activity was measured using a luminometer—Glomax 20/20 (Promega, USA).

Cell–cell fusion assay

HEK293T cells were transfected with plasmids expressing hACE2 or co-transfected with plasmids expressing SARS-COV-2 S protein (WT or mutants as mentioned) and GFP. Thirty-six hours post-transfection, both the cell lines were trypsinized and co-cultured in 1:1 ratio for 12 h followed by fixing permeabilization and subsequent imaging using fluorescence microscope (Leica Microsystems) and subsequent analysis by ImageJ software.

SARS-CoV-2 infection and drug treatment

SARS-CoV-2 (WT and different variants) and Caco-2 cells were pretreated with the appropriate posaconazole concentration for 1 h. After preincubation, cells were washed two times in serum-free medium and inoculated with the appropriate drug-treated virus, and 2 h after infection, cells were washed with complete medium, and infection allowed to proceed for the indicated time points in DMEM supplemented with 2.5% FBS and the corresponding concentration of posaconazole. Subsequently, at appropriate times post-infection, cells or supernatants were harvested and analyzed using appropriate techniques.

For more detailed description of materials and methods, see Supplementary Material Appendix.

Acknowledgments

We gratefully thank BEI resources, NIAID, and Addgene for plasmids. SARS-CoV-2-mNG was a kind gift from Dr. PEI-Yong Shi from the University of Texas Medical Branch, TX, USA. The Nano-Luciferase reporter influenza virus was a kind gift from Prof. Andrew Mehle, University of Wisconsin Madison, WI, USA.

Supplementary Material

Supplementary material is available at *PNAS Nexus* online.

Funding

This work is partly supported by the Indian Council for Medical Research (VIR/COVID-19/19/2021/ECD-I), DBT, Ramalingaswami re-entry fellowship (BT/RLF/Re-entry/02/2015), SERB, and MHRD, the "Scheme for Transformational and Advanced Research in Science" [STARS/APR2019/BS/369/FS (Project ID: 369)] awarded to A.M., Public Health Service grant R01 CA180758 to B.C., and Veterans Affairs Merit Review grant BX005490 and Research Career Scientist Awards IK6BX004212 and IK6BX003778 to S.M. and S.S.M.

Authors' Contribution

Conceptualization—A.M., A.R., and D.B. Designing experiments—A.M., A.R., I.D.J., P.B., S.B., and G.B. Performing experiments—I.D.J., A.R., P.B., S.B., K.M., A.M., G.B., S.D., A.G., S.A., S.S., and A.R.M. Manuscript writing—A.M., A.R., I.D.J., and P.B. with support from G.B., S.B., A.K.D., A.B., B.C., S.M., and S.S.M. Fund acquisition—A.M., B.C., S.M., and S.S.M.

Data Availability

All data are included in the manuscript and/or supporting information.

References

1. WHO SARS-CoV-2. 2022. https://covid19.who.int/ [accessed: 6th October 2022]
2. Mcgill AR, *et al.* 2021. SARS-CoV-2 immuno-pathogenesis and potential for diverse vaccines and therapies: opportunities and challenges. Infect Dis Rep. 13:102–125.
3. WHO SARS-CoV-2 VoCs. 2022. https://www.who.int/en/activities/tracking-SARS-CoV-2-variants/ [accessed 4 October 2022]
4. Letko M, Marzi A, Munster V. 2020. Functional assessment of cell entry and receptor usage for SARS-CoV-2 and other lineage B betacoronaviruses. Nat Microbiol. 5:562–569.
5. Hofmann H, Pöhlmann S. 2004. Cellular entry of the SARS coronavirus. Trends Microbiol. 12:466–472.
6. Huang Y, Yang C, feng Xu X, Xu W, wen Liu S. 2020. Structural and functional properties of SARS-CoV-2 spike protein: potential antivirus drug development for COVID-19. Acta Pharmacol Sin. 41:1141–1149.
7. Wrapp D, *et al.* 2020. Cryo-EM structure of the 2019-nCoV spike in the prefusion conformation. Science. 367:1260–1263.
8. Bosch BJ, van der Zee R, de Haan CAM, Rottier PJM. 2003. The coronavirus spike protein is a class I virus fusion protein: structural and functional characterization of the fusion core complex. J Virol. 77:8801–8811.
9. Xia S, *et al.* 2020. Inhibition of SARS-CoV-2 (previously 2019-nCoV) infection by a highly potent pan-coronavirus fusion inhibitor targeting its spike protein that harbors a high capacity to mediate membrane fusion. Cell Res. 30:343–355.
10. Xia S, *et al.* 2020. Fusion mechanism of 2019-nCoV and fusion inhibitors targeting HR1 domain in spike protein. Cell Mol Immunol. 17:765–767.
11. Shuai Xia LL, *et al.* 2019. A pan-coronavirus fusion inhibitor targeting the HR1 domain of human coronavirus spike. Sci Adv. 5:eaav4580.
12. a Zhu Y, Yu D, Yan H, Chong H. 2020. Design of potent membrane fusion inhibitors against SARS-CoV-2, an emerging coronavirus with fusogenic activity. J Virol. 94:1–12.
13. Zhu Y, *et al.* 2021. SARS-CoV-2-derived fusion inhibitor lipopeptides exhibit highly potent and broad-spectrum activity against divergent human coronaviruses. Signal Transduct Target Ther. 6:2020–2022.
14. Outlaw VK, *et al.* 2020. Inhibition of Coronavirus entry in vitro and ex vivo by a lipid-conjugated peptide derived from the SARS-CoV-2 spike glycoprotein HRC domain. MBio. 11:1–14.
15. Lan Q, *et al.* 2021. 25-hydroxycholesterol-conjugated EK1 peptide with potent and broad-spectrum inhibitory activity against SARS-CoV-2, its variants of concern and other human coronaviruses. Int J Mol Sci. 22:11869.
16. Fosgerau K, Hoffmann T. 2015. Peptide therapeutics: current status and future directions. Drug Discov. 20:122–128.
17. Otvos L, Wade JD. 2014. Current challenges in peptide-based drug discovery. Front Chem. 2:8–11.
18. Schlossberg D, Samuel R. 2017. NOXAFIL (Posaconazole). Antibiot Man. Second Edition: p–264-265.
19. Crawford KHD, *et al.* 2020. Protocol and reagents for pseudotyping lentiviral particles with SARS-CoV-2 spike protein for neutralization assays. Viruses. 12:513.
20. Buchrieser J, *et al.* 2020. Syncytia formation by SARS-CoV-2-infected cells. EMBO J. 39:1–12.
21. Novikov FN, Chilov GG. 2009. Molecular docking: theoretical background, practical applications and perspectives. Mendeleev Commun. 19:237–242.
22. Balaji GA, Balaji VN, Rao SN. 2013. Utility of scoring function customization in docking-based virtual screening approaches. Curr Sci. 104:86–97.
23. Morris GM, *et al.* 2009. AutoDock4 and AutoDockTools4: automated docking with selective receptor flexibility. J Comput Chem. 30:2785–2791. https:/doi.org/10.1002/jcc.21256.
24. Varela-Salinas G, García-Pérez CA, Peláez R, Rodríguez AJ. 2017. In: Visual clustering approach for docking results from vina and autodock. Martínez de Pisón FJ, Urraca R, Quintián H, Corchado E, editors. Hybrid artificial intelligent systems. La Rioja, Spain: Springer International Publishing. p. 342–353.
25. Pascarella S, *et al.* 2021. SARS-CoV-2 B.1.617 Indian variants: are electrostatic potential changes responsible for a higher transmission rate? J Med Virol. 93:6551–6556.
26. Mlcochova P, *et al.* 2021. SARS-CoV-2 B.1.617.2 Delta variant replication and immune evasion. Nature. 599:114–119.
27. Chen J, Wang R, Gilby NB, Wei G-W. 2022. Omicron variant (B.1.1.529): infectivity, vaccine breakthrough, and antibody resistance. J Chem Inf Model. 62:412–422. https:/doi.org/10.1021/acs.jcim.1c01451.
28. Plante JA, *et al.* 2021. Spike mutation D614G alters SARS-CoV-2 fitness. Nature. 592:116–121.
29. Xie X, *et al.* 2020. An infectious cDNA clone of SARS-CoV-2. Cell Host Microbe. 27:841–848.e3.
30. Weissenhorn W, *et al.* 1999. Structural basis for membrane fusion by enveloped viruses. Mol Membr Biol. 16:3–9.
31. Chambers P, Pringle CR, Easton AJ. 1990. Heptad repeat sequences are located adjacent to hydrophobic regions in several types of virus fusion glycoproteins. J Gen Virol. 71:3075–3080.
32. White JM, Delos SE, Brecher M, Schornberg K. 2008. Structures and mechanisms of viral membrane fusion proteins: multiple variations on a common theme. Crit Rev Biochem Mol Biol. 43:189–219.
33. Mzoughi O, *et al.* 2019. Trimeric heptad repeat synthetic peptides HR1 and HR2 efficiently inhibit HIV-1 entry. Biosci Rep. 39:1–15.
34. Kandeel M, *et al.* 2021. Discovery of new fusion inhibitor peptides against SARS-CoV-2 by targeting the spike S2 subunit. Biomol Ther. 29:282–289.
35. Van Dongen MJP, *et al.* 2019. A small-molecule fusion inhibitor of influenza virus is orally active in mice. Science. 363:1–28.
36. Yang C, *et al.* 2020. Salvianolic acid C potently inhibits SARS-CoV-2 infection by blocking the formation of six-helix bundle core of spike protein. Signal Transduct Target Ther. 5:2–4.
37. Bird GH, *et al.* 2014. Mucosal delivery of a double-stapled RSV peptide prevents nasopulmonary infection. J Clin Invest. 124:2113–2124.
38. Xia S, *et al.* 2018. Peptide-based membrane fusion inhibitors targeting HCoV-229E spike protein HR1 and HR2 domains. Int J Mol Sci. 19:8–11.

39. Zhu X, *et al.* 2015. Improved pharmacological and structural properties of HIV fusion inhibitor AP3 over enfuvirtide: highlighting advantages of artificial peptide strategy. Sci Rep. 5:1–15.
40. Bosch BJ, *et al.* 2004. Severe acute respiratory syndrome coronavirus (SARS-CoV) infection inhibition using spike protein heptad repeat-derived peptides. Proc Natl Acad Sci USA. 101:8455–8460.
41. Kesteleyn B, *et al.* 2017. Potent peptidic fusion inhibitors of influenza virus. Science. 2004:496–502.
42. Zhou G, *et al.* 2011. Development of indole compounds as small molecule fusion inhibitors targeting HIV-1 glycoprotein-41. J Med Chem. 23:1–7.
43. Hu X, *et al.* 2021. Discovery of small molecule entry inhibitors targeting the fusion peptide of SARS-CoV-2 spike protein. ACS Med Chem Lett. 12:1267–1274.
44. Park SB, *et al.* 2022, 2022 Jan 11. Targeting the fusion process of SARS-CoV-2 infection by small molecule inhibitors. MBio. 13. (1) https:/doi.org/10.1128/mbio.03238-21.
45. Braga L, *et al.* 2021. Drugs that inhibit TMEM16 proteins block SARS-CoV-2 spike-induced syncytia. Nature. 594: 88–93.
46. Buonaguro L, Tagliamonte M, Tornesello ML, Buonaguro FM. 2020. SARS-CoV-2 RNA polymerase as target for antiviral therapy. J Transl Med. 18:1–8.
47. Lipp HP. 2010. Clinical pharmacodynamics and pharmacokinetics of the antifungal extended-spectrum triazole posaconazole: an overview. Br J Clin Pharmacol. 70:471–480.
48. Catanzaro A, *et al.* 2007. Safety, tolerance, and efficacy of posaconazole therapy in patients with nonmeningeal disseminated or chronic pulmonary coccidioidomycosis. Clin Infect Dis. 45:562–568.
49. Patel A, Patel K, Patel K, Shah K, Chakrabarti A. 2021. Therapeutic drug monitoring of posaconazole delayed release tablet while managing COVID-19–associated mucormycosis in a real-life setting. Mycoses. 65:312–316.
50. Hatzl S, *et al.* 2020. Antifungal prophylaxis for prevention of COVID-19-associated pulmonary aspergillosis in critically ill patients: an observational study. Crit care. 25: 1–11.
51. Abidi SH, *et al.* 2021. Repurposing potential of posaconazole and grazoprevir as inhibitors of SARS-CoV-2 helicase. Sci Rep. 11: 1–11.